Construction and Building Materials 366 (2023) 130234

Contents lists available at ScienceDirect

Construction and Building Materials

journal homepage: www.elsevier.com/locate/conbuildmat

FRP-confined rubber concrete with effect of strain rate: Tests and analysis-oriented stress–strain model

Yugui Cao [a,b,c], Guoxu Zhao [a], Muyu Liu [a], Qingping Jin [d], Zhong Tao [e], Cheng Jiang [b,e,*]

[a] Hubei Key Laboratory of Roadway Bridge and Structure Engineering, Wuhan University of Technology, Wuhan 430070, China
[b] Key Laboratory of Concrete and Pre-stressed Concrete Structures of the Ministry of Education, Southeast University, Nanjing 210096, China
[c] Sanya Science and Education Innovation Park of Wuhan University of Technology, Sanya 572024, China
[d] School of Civil Engineering and Architecture, Wuhan University of Science and Technology, Wuhan 430065, China
[e] Centre for Infrastructure Engineering, Western Sydney University, Penrith, NSW 2751, Australia

ARTICLE INFO

Keywords:
FRP-confined rubber concrete
Strain rate
Lateral strain-axial strain model
Peak strength model
Stress–strain model

ABSTRACT

Rubber concrete is attracting more and more investigations and applications in recent years, due to its environmental advantages and lightweight performance. As the replacement by rubber particles can reduce the concrete strength, an efficient and lightweight solution for strengthening and repairing rubber concrete is to apply fiber-reinforced polymer (FRP) confinement. This paper is the first to consider the influence of strain rate on the stress–strain relationship of rubber concrete with FRP confinement. To develop a stress–strain model of FRP-confined rubber concrete under different strain rates, an experimental program with 36 FRP-confined concrete specimens was conducted in this work. In the experiments, rubber particles were used to replace 0–30 % fine aggregates by volume. Strain rates of 3.3×10^{-5}/s, 3.3×10^{-4}/s, and 3.3×10^{-3}/s were used to simulate three different strain rate levels of quasi-static loading, fast loading, and seismic loading, respectively. The experimental results showed that the compressive strength of FRP confined rubber concrete obviously increased with the strain rate increases, and decreased with an increasing rubber replacement ratio. Based on the experimental results, this paper proposed analytical models to predict the lateral strain-axial strain relationship, peak strength, and peak strain for FRP confined rubber concrete considering the strain rate influence. Finally, an analysis-oriented stress–strain model of FRP confined rubber concrete under different strain rates was established. The predicted results of the analysis-oriented stress–strain model showed good agreement with the experimental data.

1. Introduction

Rubber concrete is a novel type of concrete material, which uses waste tires as aggregate replacement in concrete. Rubber concrete has been widely investigated because of its good toughness, light-weight, energy dissipation, anti-impact performance, and durability. However, due to its low compressive strength and elastic modulus, rubber concrete is currently being used only for non-structural components of bridges and building structures. This greatly limits the wide application of rubber concrete in civil engineering [1–3]. Meanwhile, it is well known that wrapping fiber-reinforced polymers (FRPs) can significantly improve the mechanical behavior of normal concrete [4–12] and rubber concrete [13–15]. However, existing experimental and theoretical studies of FRP-confined rubber concrete were mainly conducted under a quasi-static loading state.

The concept of FRP confined rubber concrete is attracting increasing research interest. Chan et al. [15] experimentally studied the compressive strength of FRP confined rubber concrete. The test results showed that a compressive strength model proposed for FRP confined normal concrete could not accurately predict the compressive strength of FRP confined rubber concrete. Li et al. [16] investigated the mechanical behavior of FRP tube-encased waste tire rubber-modified concrete cylinders. Their experimental results showed that FRP could significantly improve the bearing capacity of rubber concrete, and existing compressive strength and ultimate strain models of FRP-confined ordinary concrete were not suitable for FRP-confined rubber concrete. Bompa et al. [17] experimentally studied the effect of the rubber volume content and type on the mechanical properties of FRP confined rubber

* Corresponding author.
E-mail address: cheng.jiang@westernsydney.edu.au (C. Jiang).

https://doi.org/10.1016/j.conbuildmat.2022.130234
Received 20 July 2022; Received in revised form 8 November 2022; Accepted 25 December 2022
Available online 30 December 2022

concrete under quasi-static loading and developed a stress–strain model. Cao et al. [18] showed that an FRP-confined concrete model could not accurately predict the stress–strain relationship of FRP-confined rubber concrete under cyclic axial loading, and they developed a cyclic stress–strain model for FRP-confined rubber concrete using the test data. Through a series of experiments, Youssf et al. [13,19–21] found that the confinement stress of FRP could effectively compensate for the decrease in compressive strength of rubber concrete and retained the characteristics of good ductility and seismic performance of rubber concrete.

The existing literature shows that FRP confined normal concrete is strain rate-sensitive [22–25]. In addition, Moustafa and ElGawady [26] found that FRP confined rubber concrete, where both fine and coarse aggregates were replaced by rubber, is also sensitive to strain rate. The compressive strength and ductility of FRP confined rubber concrete significantly increase with increasing strain rate. For the 3 layers of GFRP confined rubber concrete with a 20 % rubber replacement ratio, the increase in the strain rate from 2.8×10^{-5}/s to 2.8×10^{-2}/s resulted in increases in compressive strength up to 20 %. However, to the best of our knowledge, no stress–strain models have been proposed for FRP confined rubber concrete under different strain rates.

To address this research gap, this paper aims to gain a better understanding on the compressive behavior of FRP confined rubber concrete, by proposing a new stress–strain model considering the strain rate effect. Both experimental testing and analytical model were carried out. In this paper, an experiment program with 36 column specimens was conducted under different strain rates. Based on the test data, analytical models were developed to predict the lateral strain-axial strain relation, peak stress, and peak strain of FRP-confined rubber concrete. Furthermore, an analysis-oriented stress–strain model was also developed. With the proposed models, more accurate results of the mechanical behavior of FRP confined rubber concrete under compression will be obtained when analyzing and designing. It is expected that the rubber concrete will be adopted more widely benefitting from the proposed models in this paper.

2. Experimental program

2.1. Experimental design

In total, 36 specimens were prepared to study FRP confined rubber concrete under different strain rates. The size of all cylindrical specimens was 150 mm in diameter and 300 mm in height, which is widely used in studying FRP confined concrete [27–29]. Considering to avoid high strength loss, the reasonable rubber volume replacement ratio varied from 0 to 30 % in this study. The variable parameters in the test were the rubber volume replacement ratio (0 %, 20 %, and 30 %), strain rates (3.3×10^{-5}/s, 3.3×10^{-4}/s, and 3.3×10^{-3}/s), and the number of carbon FRP (CFRP) layers (1 and 2 layers). The details of both confined and unconfined specimens are summarized in Table 1, where R0, R20, and R30 in the specimen labels represent rubber volume replacement ratios of 0 %, 20 %, and 30 %, respectively; L1 and L2 denote the 1-layer and 2-layer FRPs, respectively. S1, S2, and S3 are strain rates of 3.3×10^{-5}/s, 3.3×10^{-4}/s, and 3.3×10^{-3}/s, which are used to simulate quasi-static loading, fast loading, and seismic loading, respectively [30], as shown in Fig. 1. The last letter A or B represents the first or second batch, respectively.

2.2. Material properties and concrete mix

The material properties of FRP are obtained by using the flat coupon test under different strain rates. Existing studies show that when the strain rate is lower than 3.3×10^{-3}/s, it does not obviously affect the material properties of FRP [23]. To further verify this, flat coupon tests were conducted under two strain rates of 3.3×10^{-5}/s and 3.3×10^{-3}/s. The measured material properties of FRP are listed in Table 2, which proved that the strain rate has a negligible influence on the material properties of FRP when the strain rate is in the range of 3.3×10^{-5}/s – 3.3×10^{-3}/s.

Table 1
Detail of the specimens.

Specimen ID	R_f (%)	f_{co} or f_{rc} (MPa)	ε_{co} or ε_{rc}	Strain rate (1/s)	f_{rcu} (MPa)	ε_{rcu}
R0L1S1A	0	25.4	0.002	3.3×10^{-5}	51.0	0.0205
R0L1S1B	0	24.0	0.002	3.3×10^{-5}	54.3	0.0249
R0L1S2A	0	25.4	0.002	3.3×10^{-4}	52.3	0.0216
R0L1S2B	0	24.0	0.002	3.3×10^{-4}	49.8	0.0158
R0L1S3A	0	25.4	0.002	3.3×10^{-3}	52.7	0.0200
R0L1S3B	0	24.0	0.002	3.3×10^{-3}	53.0	0.0197
R20L1S1A	20	21.0	0.0021	3.3×10^{-5}	40.7	0.0290
R20L1S1B	20	20.8	0.002	3.3×10^{-5}	46.8	0.0239
R20L1S2A	20	21.0	0.0021	3.3×10^{-4}	41.4	0.0213
R20L1S2B	20	20.8	0.002	3.3×10^{-4}	44.9	0.0215
R20L1S3A	20	21.0	0.0021	3.3×10^{-3}	46.2	0.0255
R20L1S3B	20	20.8	0.002	3.3×10^{-3}	45.7	0.0196
R30L1S1A	30	18.3	0.0026	3.3×10^{-5}	39.5	0.0267
R30L1S1B	30	17.9	0.0022	3.3×10^{-5}	39.3	0.0250
R30L1S2A	30	18.3	0.0026	3.3×10^{-4}	41.8	0.0218
R30L1S2B	30	17.9	0.0022	3.3×10^{-4}	39.3	0.0196
R30L1S3A	30	18.3	0.0026	3.3×10^{-3}	41.4	0.0214
R30L1S3B	30	17.9	0.0022	3.3×10^{-3}	40.7	0.0200
R0L2S1A	0	25.4	0.002	3.3×10^{-5}	81.0	0.0392
R0L2S1B	0	24.0	0.002	3.3×10^{-5}	76.6	0.0357
R0L2S2A	0	25.4	0.002	3.3×10^{-4}	80.6	0.0386
R0L2S2B	0	24.0	0.002	3.3×10^{-4}	76.9	0.0374
R0L2S3A	0	25.4	0.002	3.3×10^{-3}	82.2	0.0322
R0L2S3B	0	24.0	0.002	3.3×10^{-3}	78.4	0.0317
R20L2S1A	20	21.0	0.0021	3.3×10^{-5}	60.6	0.0365
R20L2S1B	20	20.8	0.002	3.3×10^{-5}	68.6	0.0398
R20L2S2A	20	21.0	0.0021	3.3×10^{-4}	59.9	0.0380
R20L2S2B	20	20.8	0.002	3.3×10^{-4}	63.7	0.0302
R20L2S3A	20	21.0	0.0021	3.3×10^{-3}	71.7	0.0323
R20L2S3B	20	20.8	0.002	3.3×10^{-3}	58.5	0.0241
R30L2S1A	30	18.3	0.0026	3.3×10^{-5}	63.3	0.0419
R30L2S1B	30	17.9	0.0022	3.3×10^{-5}	61.1	0.0409
R30L2S2A	30	18.3	0.0026	3.3×10^{-4}	–	–
R30L2S2B	30	17.9	0.0022	3.3×10^{-4}	64.6	0.0379
R30L2S3A	30	18.3	0.0026	3.3×10^{-3}	54.0	0.0346
R30L2S3B	30	17.9	0.0022	3.3×10^{-3}	63.3	0.0381

Note: R_f is the ratio of the rubber content. f_{co} and f_{rc} are the compressive strength of normal concrete and rubber concrete, respectively; ε_{co} and ε_{rc} are the peak strain of normal concrete and rubber concrete, respectively. f_{rcu} and ε_{rcu} are the ultimate stress and strain of FRP confined rubber concrete, respectively. Due to operating errors, the experimental stress–strain curve of specimen R30L2S2A was not collected.

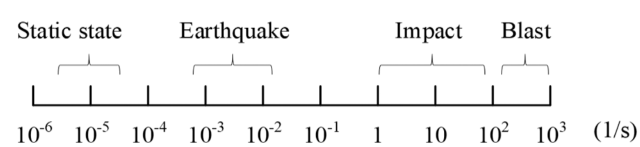

Fig. 1. Strain rates under different kinds of loads [30].

Table 2
Material properties of FRP.

Strain rate (1/s)	Thickness (mm)	Tensile strength (MPa)		Ultimate strain (%)		Elastic modulus (GPa)	
		Test	Avg	Test	Avg	Test	Avg
3.3×10^{-5}	0.167	3939	3952	1.78	1.78	220.4	221
3.3×10^{-3}	0.167	3964		1.78		221.5	

Note: "Test" denotes test value; "Avg" indicates the average value.

Normal concrete without rubber particles was prepared according to the specification for the mix proportion design of ordinary concrete [31]. In this study, river sands with a size of 0–5 mm were used as the fine aggregate, and their density was 2703 kg/m^3. Then, rubber concrete was made by partially replacing fine aggregate in concrete with a specific volume percentage of rubber particles. Waste rubber tire particles with a diameter of 1–3 mm were selected, and their density was 1119 kg/m^3. The cumulative remainder percentages for fine aggregates in the present study can be found in Fig. 2. The mix proportions of concrete with different amounts of rubber particles are listed in Table 3. It is known that the water absorption of aggregate can influence the mechanical properties of concrete. However, the rubber contents in this paper were small. Therefore, the influence of the water absorption change due to the aggregate replacement was ignored in this work.

2.3. Test setup and test program

A hydraulic servo loading device with a load capacity of 3000 kN was adopted to apply the axial load. The applied load was recorded by a load sensor placed beneath the specimen. The axial displacement was measured by four linear variable differential transformers (LVDTs), which were fixed at the middle part of the specimen, as shown in Fig. 3. To verify the measurement accuracy of the LVDTs, two strain gauges were attached vertically at the mid-height of the specimen. The lateral strain of the specimen was measured by two strain gauges, which were also attached to the specimen at the mid-height, as shown in Fig. 3. The locations of all strain gauges are also shown in Fig. 3. During the loading process, all test data were automatically collected by the data acquisition instrument.

3. Test results and discussion

3.1. Typical failure mode

The typical failure modes of FRP confined normal concrete and FRP confined rubber concrete under different strain rates are shown in Fig. 4. The specimens failed because the FRP sheet ruptured in the lateral direction, and the damage zone is mainly located at the mid-height of the specimen. The specimens tested at a loading rate of 3.3×10^{-3}/s have an obviously larger damage zone than those tested at a lower loading rate of 3.3×10^{-5}/s. However, there is no significant difference in failure severity of the specimens with different loading rates of 3.3×10^{-4}/s and 3.3×10^{-5}/s. At identical strain rates, the rubber content (0–30 %) has no significant effect on the failure severity of the specimen. This conclusion is consistent with the findings reported in a previous study [15]. The two-layer FRP-confined concrete specimens have more severe damage than the one-layer FRP-confined concrete specimens, which shows increased brittleness for specimens with an increased number of FRP layers.

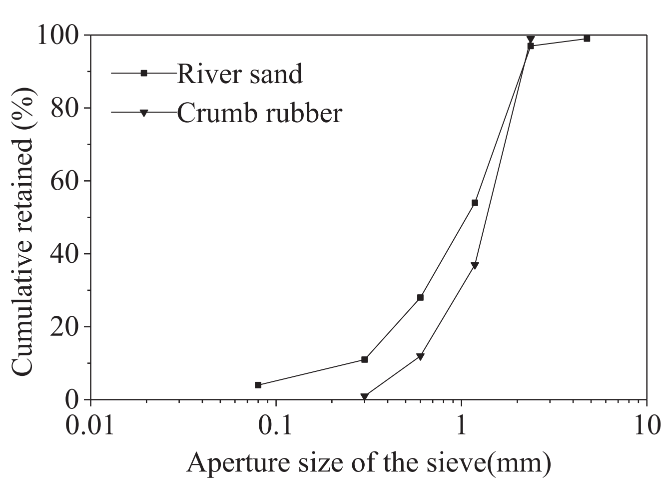

Fig. 2. Particle size distribution of fine aggregates.

Table 3
Mix proportions of concrete.

Mix code	R_f (%)	W/C	Mix proportions (kg/m^3)				
			Cement	Fine aggregate	Coarse aggregate	Water	Rubber
R0	0	0.54	350	680	1180	190	0
R20	20	0.54	350	544	1180	190	56
R30	30	0.54	350	476	1180	190	84

3.2. Axial stress-axial strain curves

Fig. 5 shows the axial stress-axial strain curves of FRP-confined rubber concrete under different strain rates. The axial stress is obtained by dividing the axial load by the cross-sectional area of the specimen, and the axial strain value is obtained from LVDT measurement. In this test, the capacity of the applied strain gauges was 0.02. When the axial strain value of the specimen exceeded 0.02, the test data measured by the strain gauge is inaccurate. Therefore, the axial strain of the specimen was measured by LVDTs to obtain global and reliable results in analysis. As can be seen in Fig. 5, the FRP-confined rubber concrete has an identical stress–strain curve shape to the FRP-confined normal concrete. When the strain rate increases, the stress–strain curves show a trend of strain hardening. Fig. 5(a) shows that the ultimate stress of specimens has an increasing trend with the strain rate increases. However, the ultimate strain decreases when the strain rate increases. This phenomenon also occurs in the studies of FRP-confined normal concrete [23]. The reason may be that the development of microcracks in the rubber concrete is delayed in the case of a higher strain rate [26]. From Fig. 5(b), it can be found that the compressive strength of the specimens with the same strain rates and FRP layer has a decreasing trend when the rubber replacement ratio increases. The reason is that the increase in rubber replacement ratio decreases the compressive strength of rubber concrete. However, the strain rate has an insignificant effect on the ultimate strain of specimens. Fig. 5 also shows that the strain rate and rubber replacement ratio have significant effects on the elastic modulus (or initial stiffness of axial stress–strain relationship). The elastic modulus value increases with the increasing strain rate, whereas decreases with the increasing rubber replacement ratio. These conclusions are identical to other existing studies [15,32].

3.3. Lateral strain-axial strain response

The lateral strain-axial strain curves of FRP-confined rubber concrete under different strain rates are shown in Fig. 6. The axial strain is obtained from the average value of the four LVDTs, while the lateral strain is obtained from the measurement of the two lateral strain gauges. Fig. 6(a) shows that the lateral strain (absolute value) is lower for the specimens with a greater rubber replacement ratio. When the axial strain is 0.02, the average lateral strains for R0 specimens, R20 specimens, and R30 specimens are 1.44 %, 1.20 %, and 1.16 %, respectively. The reason may be that specimens with higher rubber replacement ratios have relatively low strength, which leads to relatively greater confinement ratios [15]. Fig. 6(b) shows that the slope value (absolute value) of the axial strain-lateral strain curve gradually increases when the strain rate increases. In other words, at identical axial strains, a greater strain rate corresponds to a larger lateral strain and consequently a greater lateral confinement pressure provided by the FRP. This phenomenon can explain the gradual increase in compressive strength of FRP-confined concrete with increasing strain rate. A similar observation was reported by Cao et al. [23].

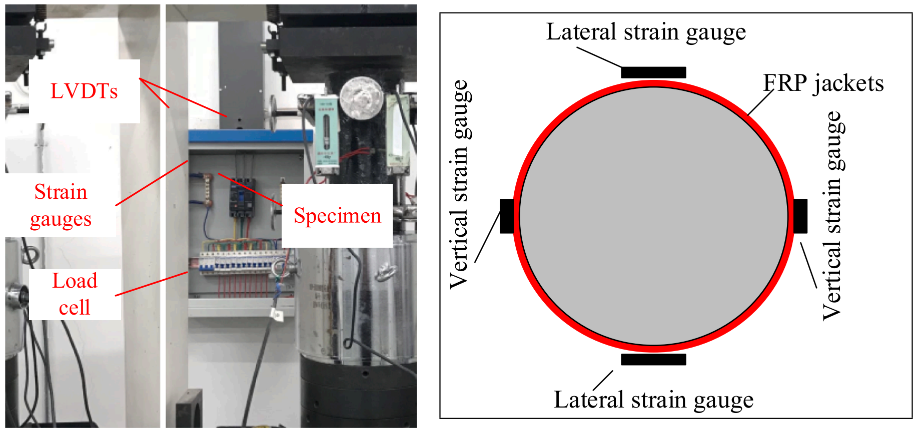

Fig. 3. Test setup.

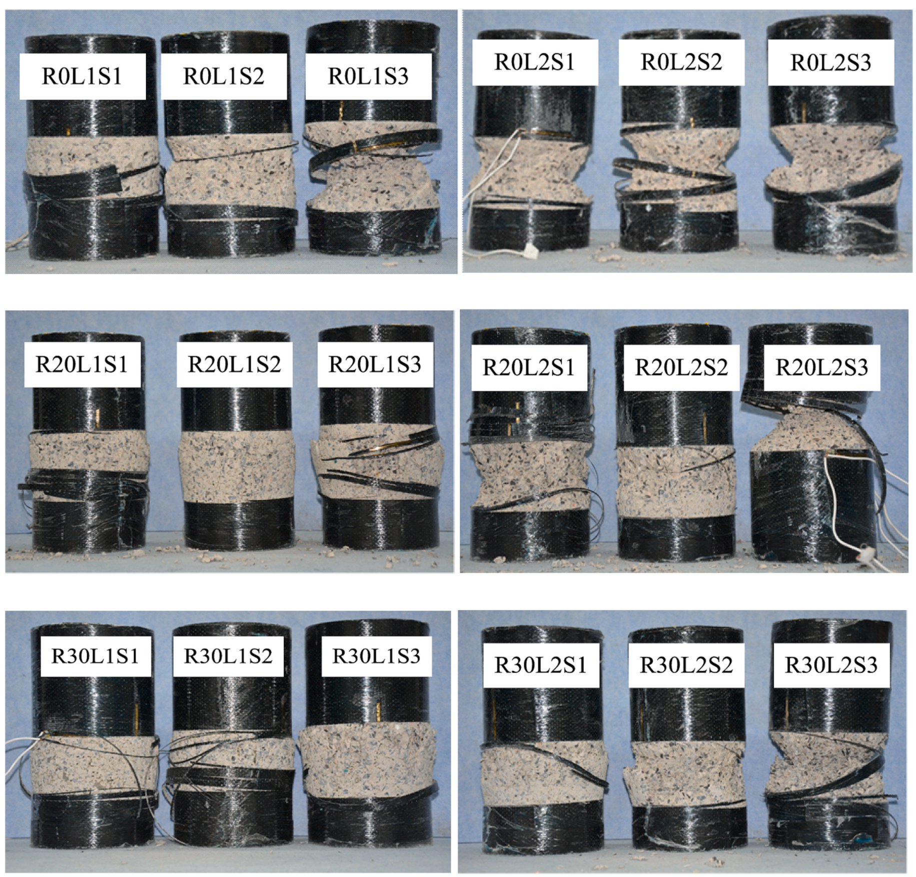

Fig. 4. Failure modes of the first batch specimens (a) Effect of strain rate (b) Effect of rubber replacement ratio.

4. Analytic stress–strain model

4.1. General description

There are many stress–strain models for FRP-confined concrete [14,33–40]. Almost all relevant analysis-oriented stress–strain models [40,41] are proposed by modifying the model of unconfined concrete [42], as shown in Eqs. (1)–(3),

$$f_c = \frac{f_{cc,\omega} x r}{r - 1 + x^r} \tag{1}$$

where

$$x = \frac{\varepsilon_c}{\varepsilon_{cc,\omega}} \tag{2}$$

$$r = \frac{E_{co}}{E_{co} - \frac{f_{cc,\omega}}{\varepsilon_{cc,\omega}}} \tag{3}$$

where ε_c is the axial strain of the concrete; E_{co} is the elastic modulus of the concrete; $f_{cc,w}$ and $\varepsilon_{cc,w}$ are the peak stress and peak strain under a certain constant confining stress, respectively.

In Eqs. (1)–(3), two key parameters ($f_{cc,w}$ and $\varepsilon_{cc,w}$) must be determined. However, according to the existing literature [41], the values of $f_{cc,w}$ and $\varepsilon_{cc,w}$ are related to the lateral strain of the FRP. Therefore, the

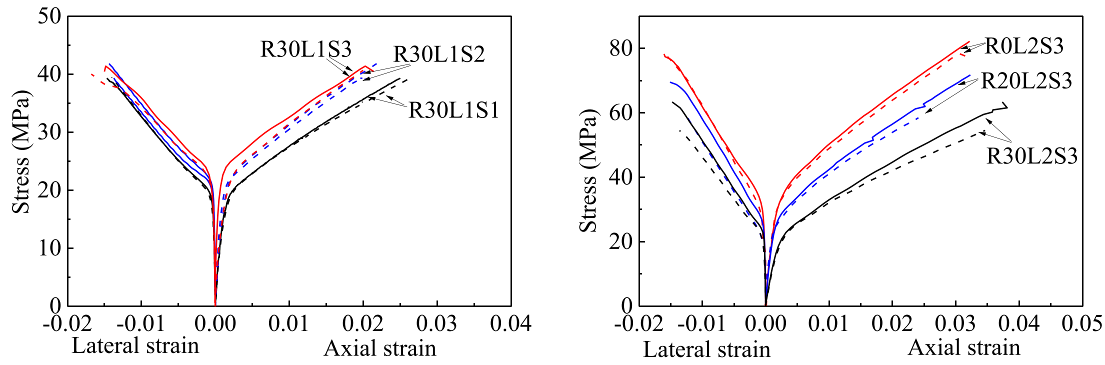

(a) Effect of strain rate (b) Effect of rubber replacement ratio

Fig. 5. The typical stress–strain curves of specimens.

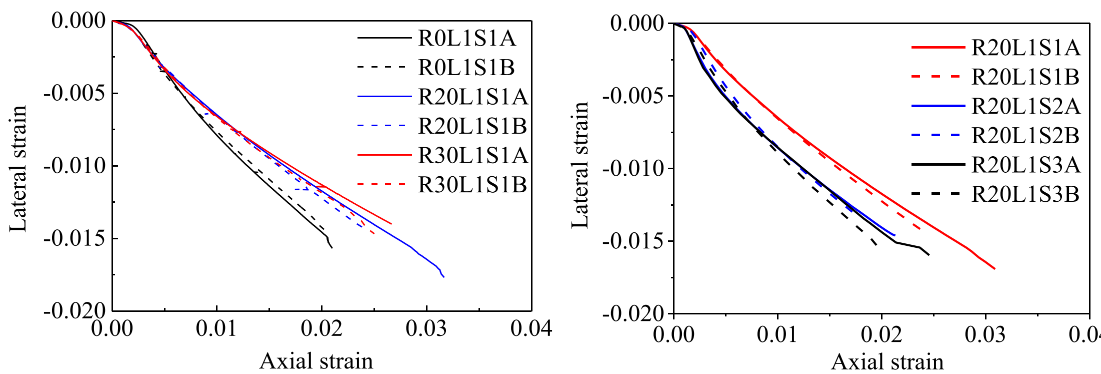

(a) Effect of rubber replacement ratio (b) Effect of strain rate

Fig. 6. The typical axial strain-lateral strain curves.

lateral strain-axial strain relationship also needs to be determined. The calculation process of those parameters is discussed as follows.

4.2. Lateral strain-axial strain model

Various existing lateral strain-axial strain models of FRP-confined concrete [35,43–45] were developed based on the model proposed by Teng et al. [37], as shown in Eq. (4). Therefore, Teng et al.'s model [37] was evaluated using the FRP-confined normal concrete data obtained in this test program, and the evaluation result is shown in Fig. 7.

$$\frac{\varepsilon_c}{\varepsilon_{co}} = 0.85\left(1+8\frac{\sigma_l}{f_{co}}\right)\left\{\left[1+0.75\left(\frac{-\varepsilon_l}{\varepsilon_{co}}\right)\right]^{0.7} - \exp\left[-7\left(\frac{-\varepsilon_l}{\varepsilon_{co}}\right)\right]\right\} \tag{4}$$

where ε_c and ε_l are the axial strain and lateral strain, respectively; f_{co} and ε_{co} are the peak stress and peak strain of normal concrete, respectively; and σ_l is the lateral stress of FRP to concrete.

The comparison in Fig. 7 shows that Teng et al.'s model [37] can accurately predict the lateral strain-axial strain relationship of FRP-confined normal concrete with different FRP layers. However, the model has not considered the effects of rubber replacement and strain rate. The experimental data in Fig. 6 clearly show that the strain rate and rubber replacement significantly affect the lateral strain-axial strain curves. Therefore, the lateral strain-axial strain relationship of FRP-confined rubber concrete under different strain rates can be obtained by modifying the model of Teng et al. [37]. The lateral strain-axial strain

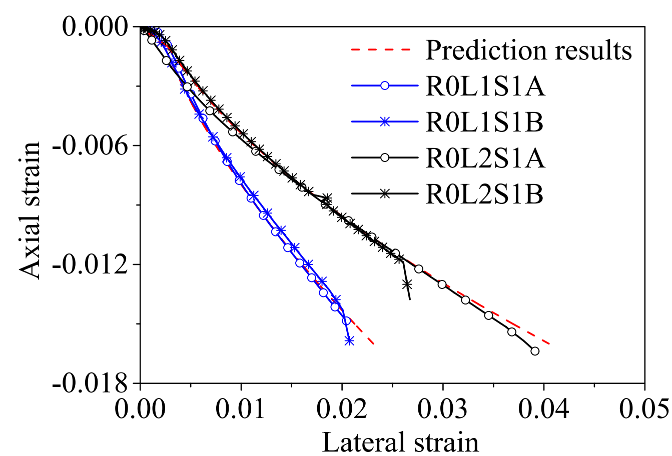

Fig. 7. Performance of Teng et al.'s model [37].

function of FRP-confined rubber concrete can be assumed as

$$\frac{\varepsilon_c}{\varepsilon_{rc}} = 0.85\left(1+8\frac{\sigma_l}{f_{rc}}\right)\left\{\left[1+0.75\left(\frac{-\varepsilon_l}{\varepsilon_{rc}}\right)\right]^{0.7} - \exp\left[-7\left(\frac{-\varepsilon_l}{\varepsilon_{rc}}\right)\right]\right\}k_R k_{vs} \tag{5}$$

$$k_R = 1 - AR_f \tag{6}$$

$$k_{vs} = 1 - B\left(\log\left(\frac{\dot{\varepsilon}}{\varepsilon_o}\right)\right)^C \tag{7}$$

where k_{vs} is the factor related to the strain rate, ε_o is the quasi-static strain rate, $\varepsilon_o = 3.3 \times 10^{-5}$/s, $\dot{\varepsilon}$ is the applied strain rate, and A, B, and C are the parameters to be determined, f_{rc} is the compressive strength of rubber concrete or normal concrete, depending on the existence of rubber aggregates. ε_{rc} is the peak strain of rubber concrete, or normal concrete, depending on the existence of rubber aggregates. By best fitting Eqs. (5)–(7) to the test data using the nonlinear fitting method, parameter values of A, B and C are obtained, which are 0.4, −0.041, and 1.56, respectively. Therefore, Eq. (5) can be rewritten as

$$\frac{\varepsilon_c}{\varepsilon_{rc}} = 0.85\left(1 + 8\frac{\sigma_l}{f_{rc}}\right)\left\{\left[1 + 0.75\left(\frac{-\varepsilon_l}{\varepsilon_{rc}}\right)\right]^{0.7} - \exp\left[-7\left(\frac{-\varepsilon_l}{\varepsilon_{rc}}\right)\right]\right\}\left(1 - 0.4R_f\right)\left[1 - 0.041\left(\log\left(\frac{\dot{\varepsilon}}{\varepsilon_o}\right)\right)^{1.56}\right] \tag{8}$$

The predictions from Eq. (8) are shown in Fig. 8. It shows that Eq. (8) can accurately predict the lateral strain-axial strain relationship of FRP-confined rubber concrete and FRP-confined normal concrete under different strain rates, respectively. It should be noted when the rubber volume replacement ratio is greater than 30 %, or the strain rate is greater than 10^{-3}/s, the accuracy of Eq. (8) needs to be further verified.

4.3. Peak stress and peak strain

4.3.1. Peak stress

Fig. 9 shows the relationship between the stress–strain curves of actively confined concrete and the stress–strain curve of FRP-confined concrete. Under identical confining stresses, the peak stress of actively confined concrete is close to the confining stress of passively confined concrete. Therefore, the compressive strength of passively confined

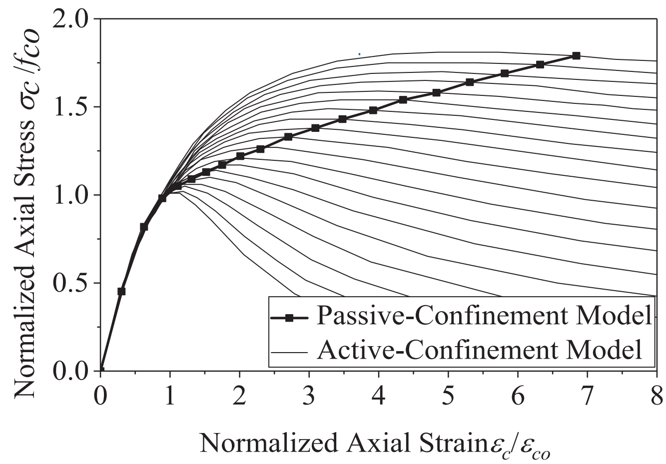

Fig. 9. Schematic calculation of the analytical model.

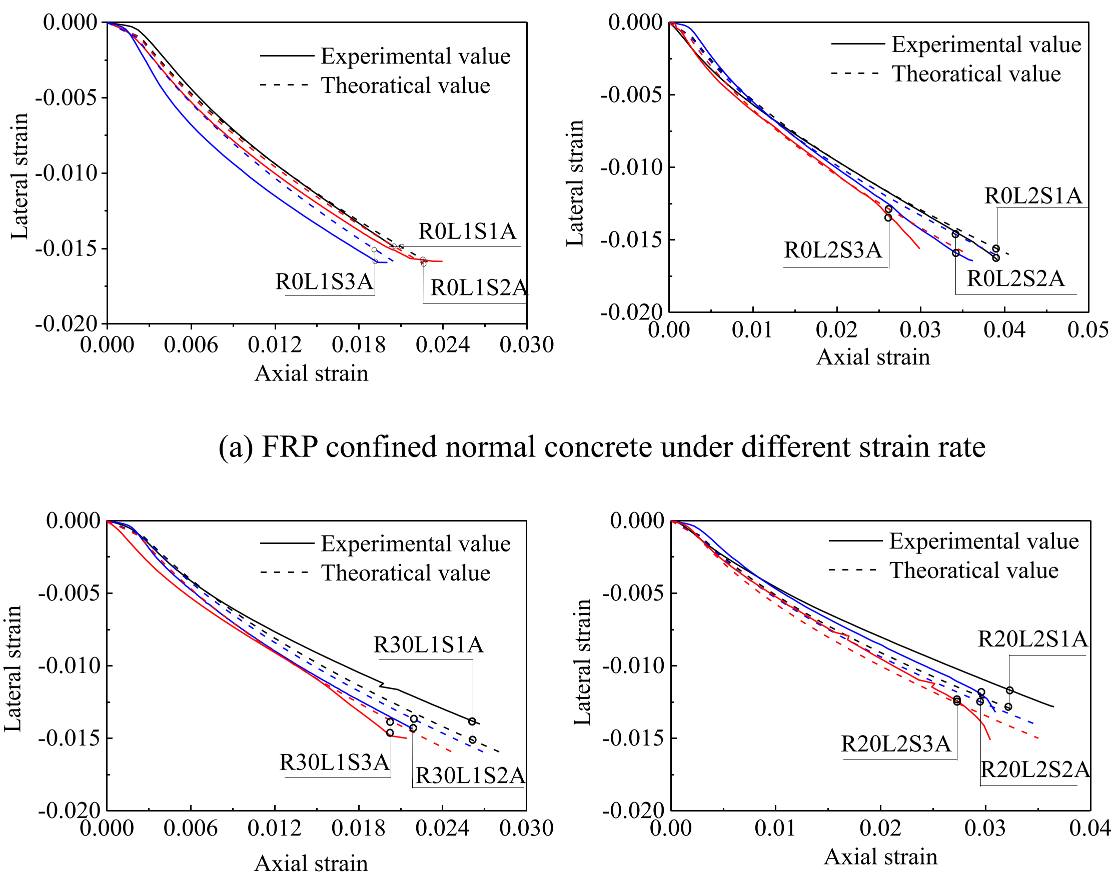

(b) FRP confined rubber concrete under different strain rate

Fig. 8. The evaluation of proposed lateral strain - axial strain model.

concrete can be used to calculate the peak stress of actively confined concrete. Related literature also reached similar conclusions [35,37,43,46]. The existing literature [47] shows that Cao et al. model [48] can accurately predict the compressive strength of FRP-confined concrete, and its expression is as follows:

$$\frac{f_{cc,w}}{f_{co}} = 1 + 8.34\left(\frac{E_l}{E_c}\right)^{1.03}\left(\frac{f_{30}}{f_{co}}\right)^{0.54}\left(\frac{\varepsilon_f}{\varepsilon_{co}}\right)^{0.82} \tag{9}$$

where E_l is the confined stiffness of FRP, E_c is the elastic modulus of FRP-confined normal concrete, f_{30} is 30 MPa, and ε_f is the rupture strain of FRP.

Fig. 10 shows that strain rates and rubber replacement ratio have significant effects on compressive strength. Compressive strength of specimens has an increasing trend with the strain rate and FRP layers increasing, and a decreasing trend with the rubber replacement ratio increases. The existing studies also obtained similar conclusions [15,26,49]. However, the influence of rubber content and loading rate is not considered in Cao et al. model [48]. Therefore, the coefficient considering rubber content R_f and the coefficient of strain rate $\lg(\dot{\varepsilon}/\varepsilon_0)$ can be added to the new model. The peak stress expression of FRP-confined rubber concrete can be written as,

$$\frac{f_{cc,w}}{f_{rc}} = \left[1 + 8.34\left(\frac{E_l}{E_{rc}}\right)^{1.03}\left(\frac{f_{30}}{f_{rc}}\right)^{0.54}\left(\frac{\varepsilon_f}{\varepsilon_{rc}}\right)^{0.82}(1 + a_3 R_f)\right]\left[1 + a_1\left(\lg\left(\frac{\dot{\varepsilon}}{\varepsilon_0}\right)\right)^{a_2}\right] \tag{10}$$

$$E_{rc} = \begin{cases} 12000\sqrt[2/3]{0.1 f_{rc}} & \text{rubber concrete} \\ 4730\sqrt{f_{rc}} & \text{normal concrete} \end{cases} \tag{11}$$

where E_{rc} is the elastic modulus of normal concrete [48] or rubber concrete [17], depending on the existence of rubber aggregates. a_1 a_2 and a_3 are coefficients that need to be determined. Coefficients a_1, a_2, and a_3 can be obtained by nonlinear regression of test data in this work, which values are 0.05, 1.00, and -0.73, respectively. Then, Eq. (10) can be rewritten as,

$$\frac{f_{cc,w}}{f_{co}} = \left[1 + 8.34\left(\frac{E_l}{E_{rc}}\right)^{1.03}\left(\frac{f_{30}}{f_{rc}}\right)^{0.54}\left(\frac{\varepsilon_f}{\varepsilon_{rc}}\right)^{0.82}(1 - 0.73 R_f)\right]\left[1 + 0.05\left(\lg\left(\frac{\dot{\varepsilon}}{\varepsilon_0}\right)\right)\right] \tag{12}$$

When the strain rate $\dot{\varepsilon}$ is equal to 3.3×10^{-5}/s and the rubber content R_f is 0, Eq. (12) becomes the compressive strength model of FRP-confined normal concrete [48]. The evaluation result of Eq. (12) is shown in Fig. 11, where AV and IAE are the error evaluation indices [50–52]. The accuracy of Eq. (12) is evaluated using these values. AV and IAE are expressed by Eqs. (13) and (14), respectively.

$$AV = \frac{1}{n}\sum_{1}^{n} Theo_i/Expe_i \tag{13}$$

$$IAE = \sum_{1}^{n}|Expe_i - Theo_i| / \sum_{1}^{n} Expe_i \tag{14}$$

where $Theo_i$ and $Expe_i$ are the i-th theoretical value and experimental value, respectively; n is the total number of test data. When the AV value is closer to 1 or IAE is closer to 0, the prediction accuracy of the model is higher. Fig. 10 shows that the AV and IAE values are 1.04 and 0.07, respectively. Therefore, Eq. (12) can be used to predict the peak stress of FRP-confined rubber concrete.

4.3.2. Peak strain

There are no existing peak strain models of FRP-confined rubber concrete under different strain rates. Based on the test data of rubberized concrete under active confinement, Gholampour et al. [53] found that the peak strain of FRP-confined rubber concrete is affected by the rubber replacement ratio and confining pressure. Moustafa [26] found that the strain rate affects the ultimate strain. Therefore, the peak strain model of actively confined rubber concrete can be written as

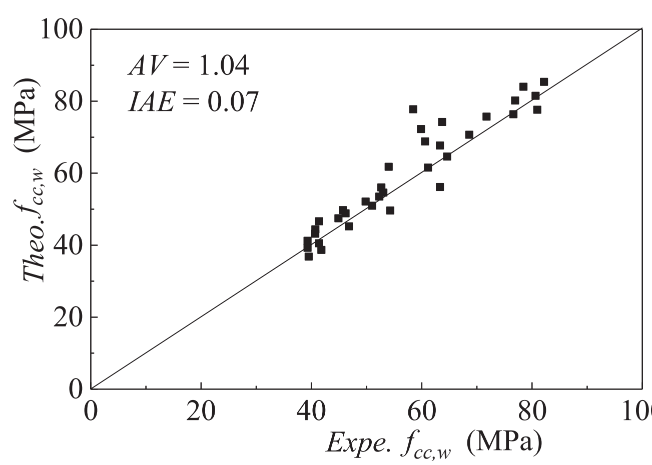

Fig. 11. Performance of the compressive strength model.

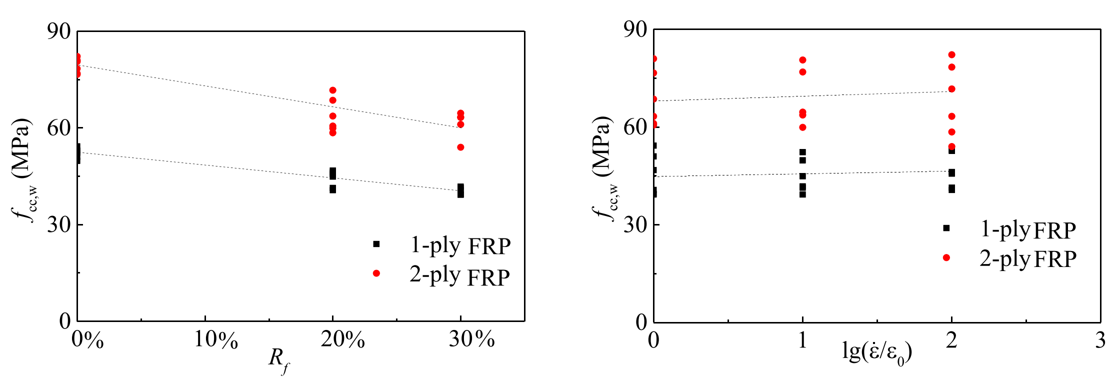

(a) Effect of rubber replacement ratio (b) Effect of different strain rate

Fig. 10. Influencing factors of compressive strength.

$$\varepsilon_{cc,w} = \varepsilon_{co}\left(1 + b_1\varphi(R_f)\left(\frac{\sigma_l}{f_{co}}\right)^{b_2}\right)\cdot k_\varepsilon \tag{15}$$

$$k_\varepsilon = 1 + b_3\left(\lg\left(\frac{\dot{\varepsilon}}{\varepsilon_0}\right)\right)^{b_4} \tag{16}$$

where b_1, b_2, b_3, and b_4 are coefficients to be determined.

To develop the peak strain model, the experimental peak strain value can be obtained using the incremental iteration method [41]. The calculation process of the experimental peak strain value is listed as follows:

(a) Use a small initial axial strain ε_c of confined concrete;
(b) Calculate the corresponding lateral strain ε_l using Eq. (8);
(c) Substitute the peak stress value $f_{cc,w}$ and experimental stress value f_c into the actively confined concrete model Eqs. (1)-(3); calculate the peak stress value $f_{cc,w}$ by Eq. (12); the experimental stress value f_c is related to the strain value ε_c in step (a);
(d) Obtain the peak strain ($\varepsilon_{cc,w}$) by solving Eq. (1);
(e) Repeat steps (a)–(c) when the calculated lateral strain ε_l is not greater than the FRP ultimate strain.
(f) Calculate the experimental peak strains of all specimens using the aforementioned processes. The program flow chart is shown in Fig. 12.

Coefficient values b_1, b_2, b_3, and b_4 in Eqs. (15) and (16) can be obtained by the regression by all experimental peak strain values. b_1, b_2, b_3, and b_4 are found to be 17.5, 1.06, −0.051, and 1.3, respectively, and Eq. (15) can be rewritten as

$$\varepsilon_{cc,w} = \varepsilon_{co}\left(1 + 17.5k_R\left(\frac{\sigma_l}{f_{co}}\right)^{1.06}\right)\cdot\left(1 - 0.051\left(\lg\left(\frac{\dot{\varepsilon}}{\varepsilon_0}\right)\right)^{1.3}\right) \tag{17}$$

When the strain rate is quasi-static loading rate and the rubber content R_f is 0, the model can be applied to normal concrete.

Due to the lack of test data of actively confined rubber concrete for modeling, the peak strain model in this work is analytically derived. While there is limited test data for actively confined rubber concrete is available for quasi-static loading cases only [53,54]. To verify the accuracy of the peak strain model in this work, the prediction results of Eq. (17) are compared with experimental data of actively confined rubber concrete under quasi-static loading [53]. The comparison results are shown in Fig. 13. It can be seen from Fig. 13 that the calculation results of Eq. (17) are very close to the test values, and the *AV* and *IAE* values are 1.1 and 0.10, respectively. This indicates the rationality of the modeling methodology in this paper.

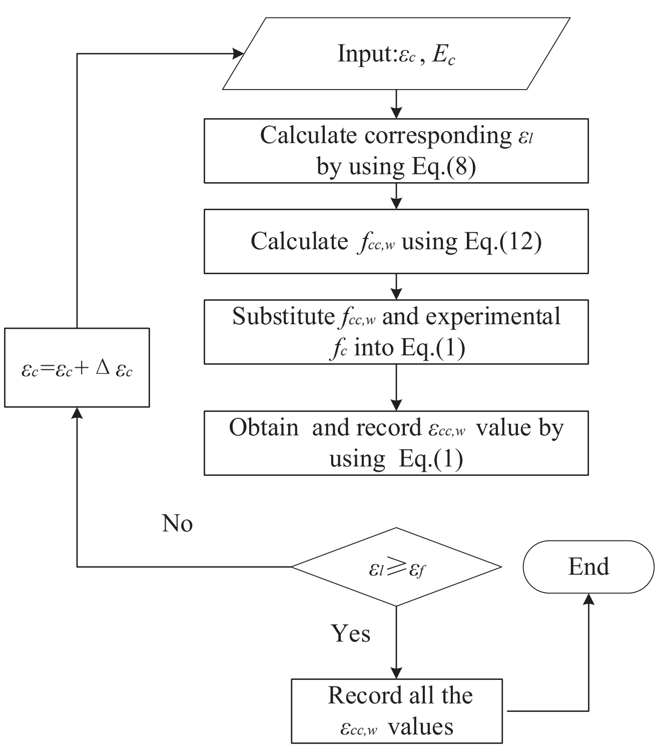

Fig. 12. Flow chart of the procedure to generate the peak axial strain.

4.3.3. Model evaluation and discussion

The stress–strain model for FRP-confined rubber concrete at different strain rates is composed of Eqs. (1), (8), (12), and (17). Fig. 14 shows the comparison results between the predicted stress–strain curves and the test curves. The comparison indicates that the proposed stress–strain model has good performance.

The newly established analytical stress–strain relationship model includes two factors: rubber replacement ratio R_f and strain rate. When the rubber replacement ratio R_f is 0, the newly proposed model can predict the stress–strain curve of FRP-confined normal concrete with different strain rates. When the strain rate is 0, the newly proposed model can predict the stress–strain curves of the FRP-confined rubber concrete under a quasi-static strain rate. The accuracy of the newly established model was verified using data from published literature [15,23], and the results are shown in Fig. 15. The comparison indicates that the proposed model also has good performance in predicting the stress–strain curves of the FRP-confined rubber concrete under quasi-static strain rate, or FRP-confined normal concrete with different strain rates.

5. Conclusions

In this paper, the mechanical behavior of FRP-confined rubber concrete under different strain rates was examined using 36 tested specimens. Based on the test results and analytical study in this paper, the following conclusions can be drawn:

(1) All the specimens failed by FRP rupture with concrete damage. The damage severity of concrete is greatly affected by the loading rate and the number of FRP layers. The rubber content has no obvious effect on the damage severity. When the loading rate or the number of FRP layers increases, the damage becomes more obvious.
(2) The slope of the lateral strain-axial strain curve of FRP-confined rubber concrete increases with higher strain rates. The existing lateral strain-axial strain relationship model proposed for

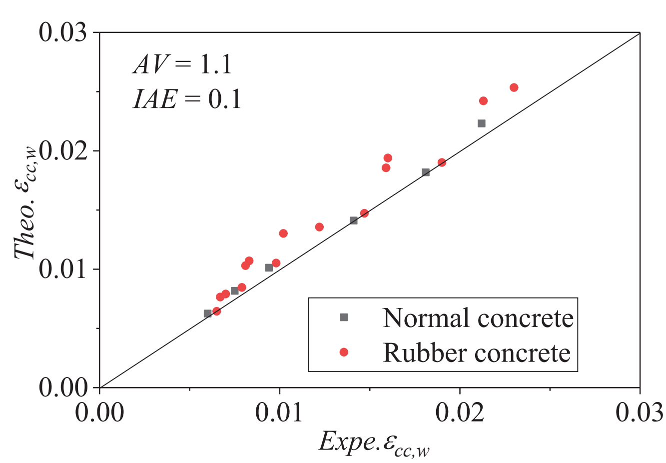

Fig. 13. Evaluation of Eq. (17).

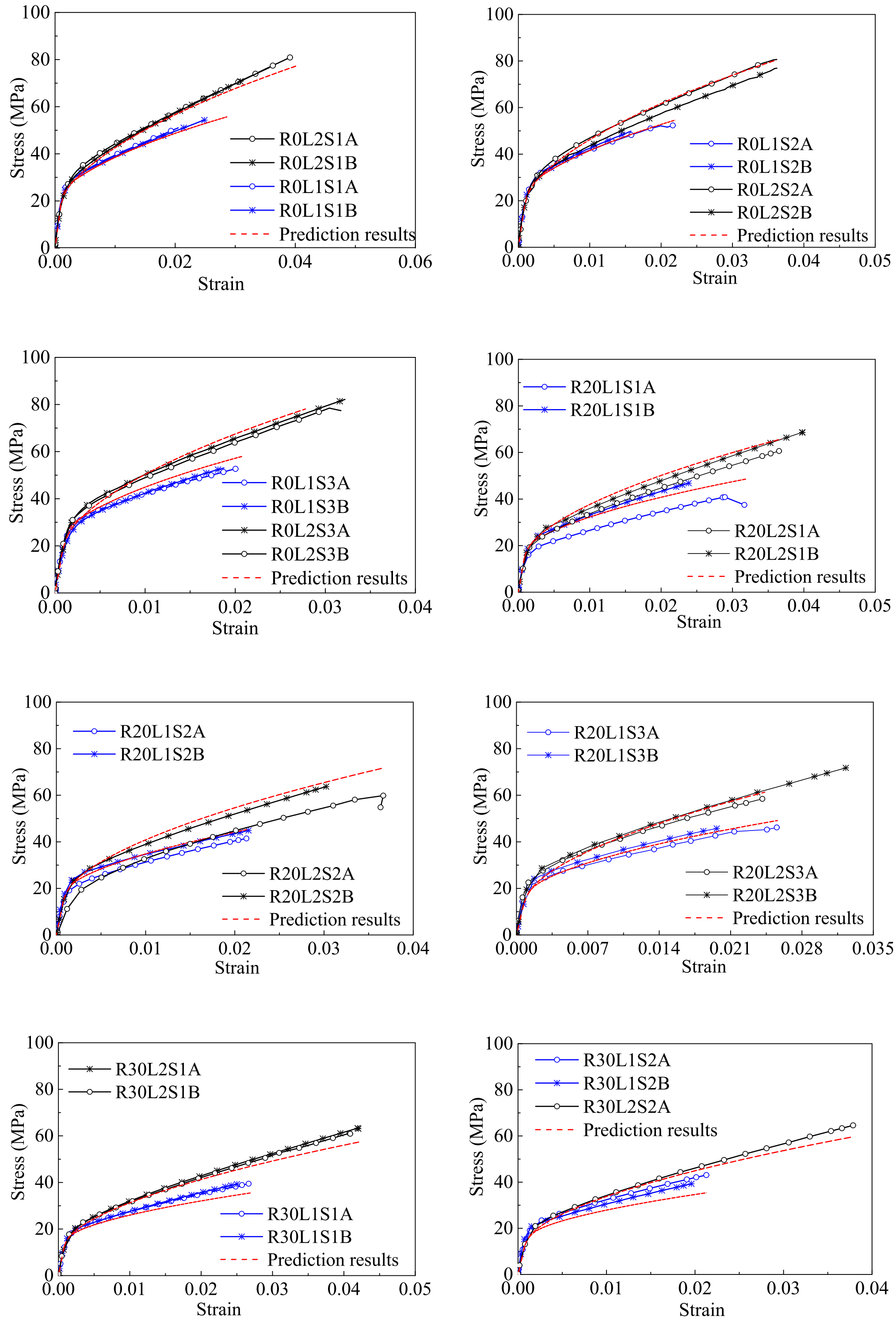

Fig. 14. Evaluation of the proposed model with test data in this work.

conventional FRP-confined concrete is not applicable for FRP-confined rubber concrete. A new model was proposed accordingly in this paper, which can accurately reflect the lateral strain-axial strain relationship of FRP-confined rubber concrete under different strain rates.

(3) A new analysis-oriented stress–strain model of FRP-confined rubber concrete under different strain rates is proposed, and the model can accurately predict the test data. This model can be used for both FRP-confined rubber concrete and FRP-confined normal concrete.

(4) Future research will be carried out for FRP-confined concrete specimens with rubber volume replacement ratio greater than 30 %, and strain rate greater than 3.3×10^{-3}/s.

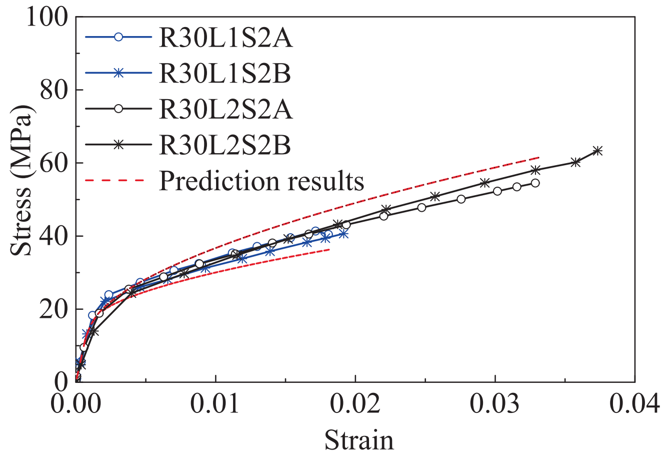

Fig. 14. (*continued*).

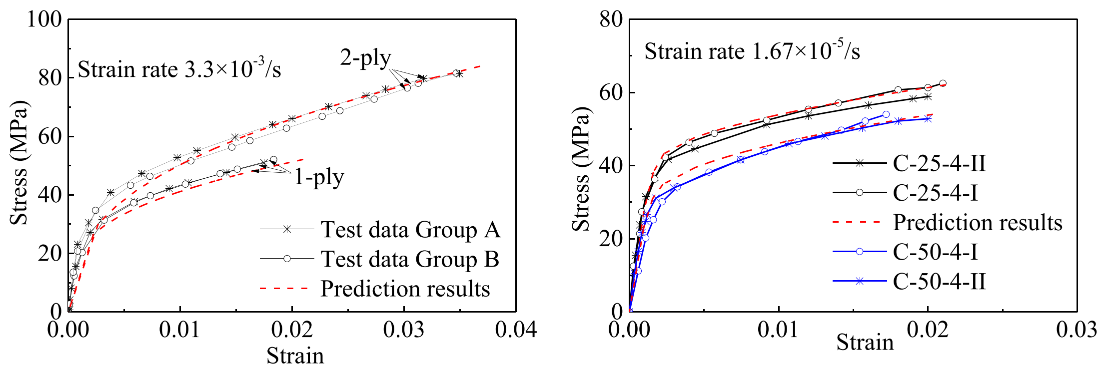

(a) FRP confined normal concrete [23] (b) FRP confined rubber concrete [15]

Fig. 15. Evaluation of the proposed model using existing test data.

CRediT authorship contribution statement

Yugui Cao: Conceptualization, Methodology, Formal analysis, Investigation, Writing – review & editing, Validation. **Guoxu Zhao:** Writing – original draft. **Muyu Liu:** Supervision. **Qingping Jin:** Investigation. **Zhong Tao:** Writing – review & editing, Supervision. **Cheng Jiang:** Methodology, Supervision, Writing – review & editing.

Declaration of Competing Interest

The authors declare that they have no known competing financial interests or personal relationships that could have appeared to influence the work reported in this paper.

Data availability

Data will be made available on request.

Acknowledgements

This study was funded by the National Natural Science Foundation of China (Grant No. 51808419), the Hubei Key Laboratory of Roadway Bridge and Structure Engineering (Wuhan University of Technology) (Grant No. DQJJ201901, DQJJ202103), Sanya Science and Education Innovation Park of Wuhan University of Technology (Grant No. 2021KF005) and Australian Research Council (DE210101662), for which the authors are grateful. At the same time, the authors also thank the Master students Li Longlong, Hou Can, Zhang Yang, and Wu Feng for their assistance during the experiment.

References

[1] S.M.S. Kazmi, M.J. Munir, Y.F. Wu, Application of waste tire rubber and recycled aggregates in concrete products: A new compression casting approach, Resources, Conserv Recy 167 (2021), 105353.
[2] J. Xie, J. Li, Z. Lu, Z. Li, C. Fang, L. Huang, L. Li, Combination effects of rubber and silica fume on the fracture behaviour of steel-fibre recycled aggregate concrete, Constr Build Mater 203 (2019) 164–173.
[3] X. Li, T.C. Ling, K.H. Mo, Functions and impacts of plastic/rubber wastes as eco-friendly aggregate in concrete–A review, Constr Build Mater 240 (2020), 117869.
[4] L.J. Ouyang, M.X. Chai, J. Song, et al., Repair of thermally damaged concrete cylinders with basalt fiber-reinforced polymer jackets, J Build Eng 44 (2021), 102673.
[5] I. Tijani, C. Jiang, C. Lim, Y.F. Wu, Effect of load eccentricity on the mechanical response of FRP-confined predamaged concrete under compression, J Compos Constr 24 (5) (2020) 04020057.
[6] Y.F. Wu, Y.G. Cao, Effect of load path on behavior of FRP-confined concrete, J Compos Constr 21 (4) (2017) 04017014.
[7] J. Liao, J.J. Zeng, C. Jiang, J.X. Li, J.S. Yuan, Stress-strain behavior and design-oriented model for FRP spiral strip-confined concrete, Compos Struct 293 (2022), 115747.
[8] Y.R. Zhang, Y. Wei, B. Li, G.F. Wang, L.J. Huang, A novel seawater and sea sand concrete-filled FRP-carbon steel composite tube column: seismic behavior and finite-element analysis, Eng Struct 270 (2022), 114872.
[9] Wei Y, Zhu C Miao KT, Chai J, Zheng KQ. Compressive behavior of rectangular concrete-filled fiber-reinforced polymer and steel composite tube columns with stress-release grooves. Compos Struct 2022; 281:114984.
[10] C. Jiang, Strength enhancement due to FRP confinement for coarse aggregate-free concretes, Eng Struct 277 (2023), 115370.

[11] I.A. Tijani, C. Jiang, C. Lim, Y.F. Wu, Eccentrically loaded concrete under nonuniform passive confinement, J Struct Eng 148 (2022) 04021247.
[12] C. Jiang, F. Yuan, Y.F. Wu, X.M. Zhao, Effect of interfacial bond on plastic hinge length of FRP-confined RC columns, J Compos Constr 23 (2019) 04019007.
[13] O. Youssf, M.A. ElGawady, J.E. Mills, Static cyclic behaviour of FRP-confined crumb rubber concrete columns, Eng Struct 113 (2016) 371–387.
[14] S. Raffoul, D. Escolano-Margarit, R. Garcia, M. Guadagnini, K. Pilakoutas, Constitutive model for rubberized concrete passively confined with FRP laminates, J Compos Constr 23 (6) (2019) 04019044.
[15] C.W. Chan, T. Yu, S. Zhang, Q. Xu, Compressive behaviour of FRP-confined rubber concrete, Constr Build Mater 211 (2019) 416–426.
[16] G. Li, S.S. Pang, S.I. Ibekwe, FRP tube encased rubberized concrete cylinders, Mater Struct 44 (1) (2011) 233–243.
[17] D.V. Bompa, A.Y. Elghazouli, Stress-strain response and practical design expressions for FRP-confined recycled tyre rubber concrete, Constr Build Mater 237 (2020), 117633.
[18] Y. Cao, L. Li, M. Liu, Y. Wu, Mechanical behavior of FRP confined rubber concrete under monotonic and cyclic loading, Compos Struct 114205 (2021).
[19] M.N. Youssef, M.Q. Feng, A.S. Mosallam, Stress-strain model for concrete confined by FRP composites, Compos B Eng 38 (5) (2007) 614–628.
[20] O. Youssf, M.A. Elgawady, J.E. Mills, X. Ma, An experimental investigation of crumb rubber concrete confined by fibre reinforced polymer tubes, Constr Build Mater 53 (4) (2014) 522–532.
[21] O. Youssf, R. Hassanli, J.E. Mills, Mechanical performance of FRP-confined and unconfined crumb rubber concrete containing high rubber content, J Build Eng 11 (2017) 115–126.
[22] Y.L. Bai, Z.W. Yan, T. Ozbakkaloglu, W.Y. Gao, J.J. Zeng, Mechanical behavior of large-rupture-strain (LRS) polyethylene naphthalene fiber bundles at different strain rates and temperatures, Constr Build Mater 297 (2021), 123786.
[23] Y. Cao, M. Liu, Y.F. Wu, Effect of low strain rate on the axial behavior of concrete in CFRP-confined circular cylinders, Constr Build Mater 255 (2020), 119351.
[24] Y. Cao, M. Liu, Y. Zhang, J. Hu, S. Yang, Effect of strain rates on the stress-strain behavior of FRP-confined pre-damaged concrete, Materials 13 (5) (2020) 1078.
[25] Z.W. Yan, Y.L. Bai, T. Ozbakkaloglu, et al., Rate-dependent compressive behavior of concrete confined with large-rupture-strain (LRS) FRP, Compos Struct 272 (2021), 114199.
[26] A. Moustafa, M.A. ElGawady, Strain rate effect on properties of rubberized concrete confined with glass fiber-reinforced polymers, J Compos Constr 20 (5) (2016) 04016014.
[27] Y.F. Wu, C. Jiang, Effect of load eccentricity on the stress-strain relationship of FRP-confined concrete columns, Compos Struct 98 (2013) 228–241.
[28] C. Jiang, Y.F. Wu, Axial strength of eccentrically loaded FRP-confined short concrete columns, Polymers 12 (6) (2020) 1261.
[29] Y. Cao, Y.F. Wu, C. Jiang, Stress-strain relationship of FRP confined concrete columns under combined axial load and bending moment, Compos B Eng 134 (2018) 207–217.
[30] P.H. Bischoff, S.H. Perry, Compressive behaviour of concrete at high strain rates, Mater Struct 24 (6) (1991) 425–450.
[31] C. Standard, JGJ 55–2011, China Architecture and Building Press, Beijing, Specification for mix proportion design of ordinary concrete, 2011 in Chinese.
[32] D.V. Bompa, A.Y. Elghazouli, Behaviour of confined rubberised concrete members under combined loading conditions, Mag. Concr. Res. 1–19 (2019).
[33] J.G. Teng, G. Lin, T. Yu, Analysis-oriented stress-strain model for concrete under combined FRP-steel confinement, J Compos Constr 19 (5) (2015) 04014084.
[34] Y. Pan, R. Guo, H. Li, et al., Analysis-oriented stress-strain model for FRP-confined concrete with preload, Compos Struct 166 (2017) 57–67.
[35] T. Jiang, J.G. Teng, Analysis-oriented stress-strain models for FRP-confined concrete, Eng Struct 29 (11) (2007) 2968–2986.
[36] F. Braga, R. Gigliotti, M. Laterza, Analytical stress-strain relationship for concrete confined by steel stirrups and/or FRP jackets, J Struct Eng 132 (9) (2006) 1402–1416.
[37] J.G. Teng, Y.L. Huang, L. Lam, L.P. Ye, Theoretical model for fiber-reinforced polymer-confined concrete, J Compos Constr 11 (2) (2007) 201–210.
[38] Y.L. Li, J.G. Teng, X.L. Zhao, R.K.S. Raman, Theoretical model for seawater and sea sand concrete-filled circular FRP tubular stub columns under axial compression, Eng Struct 160 (2018) 71–84.
[39] T.A. Hales, C.P. Pantelides, P. Sankholkar, et al., Analysis-oriented stress-strain model for concrete confined with fiber-reinforced polymer spirals, ACI Struct J 114 (5) (2017) 1263–1272.
[40] M.F. Ferrotto, O. Fischer, L. Cavaleri, Analysis-oriented stress-strain model of CRFP-confined circular concrete columns with applied preload, Mater Struct 51 (2) (2018) 1–16.
[41] Y.G. Cao, Y. Zhang, M.Y. Liu, Z.F. Lu, C. Jiang, Analysis-oriented stress-strain model for FRP-confined predamaged concrete, J Build Eng 36 (2021), 102121.
[42] S. Popovics, A numerical approach to the complete stress-strain curve of concrete, Cem Concr Res 3 (5) (1973) 583–599.
[43] T. Ozbakkaloglu, J.C. Lim, T. Vincent, FRP-confined concrete in circular sections: Review and assessment of stress-strain models, Eng Struct 49 (2013) 1068–1088.
[44] A. Kwan, C. Dong, J. Ho, Axial and lateral stress-strain model for FRP confined concrete, Eng Struct 99 (2015) 285–295.
[45] J.C. Lim, T. Ozbakkaloglu, Lateral strain-to-axial strain relationship of confined concrete, J Struct Eng 141 (5) (2014) 04014141.
[46] T. Vincent, T. Ozbakkaloglu, Influence of concrete strength and confinement method on axial compressive behavior of FRP confined high-and ultra high-strength concrete, Compos B Eng 50 (2013) 413–428.
[47] N. Diboune, R. Benzaid, M. Berradia, New strength-strain model and stress-strain relationship for square and rectangular concrete columns confined with CFRP wraps, Mech. Adv. Mater. Struct. 1–24 (2022).
[48] Y.G. Cao, C. Jiang, Y.F. Wu, Cross-Sectional Unification on the Stress-Strain Model of Concrete Subjected to High Passive Confinement by Fiber-Reinforced Polymer, Polymers 8 (2016) 186.
[49] L. Zheng, X.S. Huo, Y. Yuan, Strength, modulus of elasticity, and brittleness index of rubberized concrete, J Mater Civil Eng 20 (11) (2008) 692–699.
[50] Y. Wei, X. Zhang, G. Wu, Y. Zhou, Behaviour of concrete confined by both steel spirals and fiber-reinforced polymer under axial load, Compos Struct 192 (2018) 577–591.
[51] Y.G. Cao, C. Hou, M.Y. Liu, C. Jiang, Effects of predamage and load cyclic on compression behavior of fiber reinforced polymer-confined concrete, Struct Concrete 22 (3) (2021) 1784–1799.
[52] Y. Wei, C. Jiang, Y.F. Wu, Confinement effectiveness of circular concrete-filled steel tubular columns under axial compression, J Constr Steel Res 158 (2019) 15–27.
[53] A. Gholampour, T. Ozbakkaloglu, R. Hassanli, Behavior of rubberized concrete under active confinement, Constr Build Mater 138 (2017) 372–382.
[54] A. Gholampour, A. Fallah Pour, R. Hassanli, T. Ozbakkaloglu, Behavior of actively confined rubberized concrete under cyclic axial compression, J Struct Eng 145 (2019) 04019131.